

Tunable thermal conductivity and mechanical properties of metastable silicon by phase engineering

Guoshuai Du(杜国帅), Yubing Du(杜玉冰), Jiaxin Ming(明嘉欣), Zhixi Zhu(朱芷希), Jiaohui Yan(闫皎辉), Jiayin Li(李嘉荫), Tiansong Zhang(张天颂), Lina Yang(杨哩娜), Ke Jin(靳柯), and Yabin Chen(陈亚彬)

Citatio: Chin. Phys. B, 2025, 34 (**9**): 096401. DOI: 10.1088/1674-1056/adcf8a
http://cpb.iphy.ac.cn; http://iopscience.iop.org/cpb

What follows is a list of articles you may be interested in

Thermal investigation of water-based radiative magnetized micropolar hybrid nanofluid flow subject to impacts of the Cattaneo-Christov flux model on a variable porous stretching sheet with a machine learning approach

Showkat Ahmad Lone, Zehba Raizah, Rawan Bossly, Fuad S. Alduais, Afrah Al-Bossly, and Arshad Khan
Chin. Phys. B, 2025, 34 (**6**): 064401. DOI: 10.1088/1674-1056/adc65e

Anomalous bond-length behaviors of solid halogens under pressure

Min Wu(吴旻), Ye-Feng Wu(吴烨峰), and Yi Ma(马毅)
Chin. Phys. B, 2021, 30 (**7**): 076401. DOI: 10.1088/1674-1056/abf4bd

Unraveling the effect of uniaxial strain on thermoelectric properties of Mg_2Si: A density functional theory study

Kulwinder Kaur, Ranjan Kumar
Chin. Phys. B, 2017, 26 (**6**): 066401. DOI: 10.1088/1674-1056/26/6/066401

Secondary relaxation and dynamic heterogeneity in metallic glasses: A brief review

J C Qiao(乔吉超), Q Wang, D Crespo, Y Yang(杨勇), J M Pelletier
Chin. Phys. B, 2017, 26 (**1**): 016402. DOI: 10.1088/1674-1056/26/1/016402

First principle investigation of the electronic and thermoelectric properties of Mg_2C

Kulwinder Kaur, Ranjan Kumar
Chin. Phys. B, 2016, 25 (**2**): 026402. DOI: 10.1088/1674-1056/25/2/026402

SPECIAL TOPIC — Heat conduction and its related interdisciplinary areas

Tunable thermal conductivity and mechanical properties of metastable silicon by phase engineering

Guoshuai Du(杜国帅)[1,2,†], Yubing Du(杜玉冰)[1,2,†], Jiaxin Ming(明嘉欣)[1,3], Zhixi Zhu(朱芷希)[4], Jiaohui Yan(闫皎辉)[4], Jiayin Li(李嘉荫)[1,3], Tiansong Zhang(张天颂)[1,2], Lina Yang(杨哩娜)[2,§], Ke Jin(靳柯)[1,4], and Yabin Chen(陈亚彬)[1,2,5,‡]

[1] *Advanced Research Institute of Multidisciplinary Sciences (ARIMS), Beijing Institute of Technology, Beijing* 100081, *China*
[2] *School of Aerospace Engineering, Beijing Institute of Technology, Beijing* 100081, *China*
[3] *School of Chemistry and Chemical Engineering, Beijing Institute of Technology, Beijing* 100081, *China*
[4] *School of Materials Science and Engineering, Beijing Institute of Technology, Beijing* 100081, *China*
[5] *Beijing Institute of Technology Chongqing Institute of Microelectronics and Microsystems, Chongqing* 400030, *China*

(Received 13 March 2025; revised manuscript received 8 April 2025; accepted manuscript online 23 April 2025)

The extensive applications of cubic silicon in flexible transistors and infrared detectors are greatly hindered by its intrinsic properties. Metastable silicon phases, such as Si-III, IV, and XII, prepared using extreme pressure methods, provide a unique "genetic bank" with diverse structures and exotic characteristics. However, exploration of their inherent physical properties remains underdeveloped. Herein, we demonstrate the phase engineering strategy to modulate the thermal conductivity and mechanical properties of metastable silicon. The thermal conductivity, obtained via the Raman optothermal approach, exhibits broad tunability across various Si-I, III, XII, and IV phases. The hardness and Young's modulus of Si-IV are significantly greater than those of the Si-III/XII mixture, as confirmed by the nanoindentation technique. Moreover, it was found that pressure-induced structural defects can substantially degrade the thermal and mechanical properties of silicon. This systematic investigation offers a feasible route for designing novel semiconductors and further advancing their desirable applications in advanced nanodevices and mechanical transducers.

Keywords: metastable silicon, thermal conductivity, mechanical property, high pressure

PACS: 64.60.My, 74.25.Fc, 62.20.−x, 07.35.+k

DOI: 10.1088/1674-1056/adcf8a **CSTR:** 32038.14.CPB.adcf8a

1. Introduction

As the key component of integrated circuits and photovoltaics, cubic silicon (Si-I) has attracted extensive attention in the semiconductor industry over the past few decades, owing to its superior electronic and optical properties.[1–4] Further applications of Si-I are significantly impeded by its intrinsic properties, such as in infrared photodetectors and flexible nanodevices.[5] Metastable silicon, synthesized by high-pressure treatment, has emerged as a promising alternative to offer enhanced properties compared to Si-I.[6] It has been found that Si can undergo several phase transitions under hydrostatic or uniaxial pressure, including the metallic Si-II (β-Sn), Si-XI (*Imma*), Si-V (hexagonal), Si-VI (*Cmca*), Si-VII (hcp), and Si-X (fcc) phases.[7–9] Intriguingly, upon decompression, tetragonal Si-II can irreversibly transform into the mixed Si-XII (R8) and Si-III (BC8) phases, rather than returning to the initial Si-I phase, and the latter can then become hexagonal Si-IV through thermal annealing.[10] Despite considerable efforts, the intrinsic thermal and mechanical properties of these metastable phases remain largely unexplored.[11–16]

Metastable silicon phases provide a versatile platform to modulate their thermal properties and phonon transport behaviors.[17] First-principles calculations combined with Boltzmann transport theory indicate that the thermal conductivity of rhombohedral Si-XII (16.8 $\mathrm{W{\cdot}m^{-1}{\cdot}K^{-1}}$) is about one order of magnitude lower than that of cubic Si-I (144 $\mathrm{W{\cdot}m^{-1}{\cdot}K^{-1}}$), attributed to its stronger three-phonon scattering.[18] The thermal conductivity of body-centered Si-III, prepared through direct transformation using the multi-anvil method, was determined to be 20 $\mathrm{W{\cdot}m^{-1}{\cdot}K^{-1}}$ at room temperature,[15] although the intrinsic physical properties of Si-III remain contentious. In practice, a Si-III/XII mixture normally coexists when metallic Si-II is fully decompressed, due to their equivalent potential energy, yielding variable thermal conductivity from 7.6 $\mathrm{W{\cdot}m^{-1}{\cdot}K^{-1}}$ to 22.2 $\mathrm{W{\cdot}m^{-1}{\cdot}K^{-1}}$ as measured by the time-domain thermoreflectance technique.[19] Additionally, the thermal properties of

†These authors contributed equally to this work.
‡Corresponding author. E-mail: chyb0422@bit.edu.cn
§Corresponding author. E-mail: yangln@bit.edu.cn

© 2025 Chinese Physical Society and IOP Publishing Ltd. All rights, including for text and data mining, AI training, and similar technologies, are reserved.

the hexagonal Si-IV phase are still unclear, and first-principles calculations show its thermal conductivity to be about 40% lower than that of cubic Si-I.[20]

Investigations into the mechanical properties of metastable Si phases remain in their infancy, to the best of our knowledge. It has been found that the elastic modulus (152 GPa) and hardness (12.0 GPa) of the polycrystalline Si-IV phase are similar to those of cubic Si-I, as confirmed by nanoindentation and x-ray diffraction.[21] Notably, the Si-IV phase can display various polytypes depending on their stacking orders, such as 2H (AB stacking) and 4H (ABCB stacking) structures.[13] Moreover, the elastic modulus of high-quality Si crystals can be significantly weakened when numerous structural defects appear, such as grain boundary, triple line junction and quadratic node, which has been theoretically demonstrated using Budiansky's self-consistent method together with a phase mixture model.[22] Clearly, experimental determination of the mechanical properties of metastable Si phases is highly desirable for their potential applications in flexible devices and advanced mechanical sensors.

In this study, both thermal and mechanical properties of metastable Si-III/XII and Si-IV phases, as well as decompressed polycrystalline Si-I, have been comprehensively investigated. The measured thermal conductivity using the Raman optothermal approach exhibits broad tunability across different metastable phases. The phase dependence of hardness and elastic modulus of silicon phases has been developed based on continuous stiffness measurements via the nanoindentation technique. Moreover, pressure-induced structural defects play a crucial role in the phonon scattering process, resulting in significantly degraded thermal and mechanical properties. It is anticipated that the discoveries in this work will lay a solid foundation for the potential applications of metastable silicon phases.

2. Experimental methods

Different phase structures of Si were prepared through high-pressure and thermal annealing treatments. First, the Si-I phase was compressed to around 12 GPa to induce a phase transition to the Si-II phase. Upon decompression back to ambient pressure, the Si-III/XII phase was obtained. Annealing the Si-III/XII phase at approximately 470 K led to the formation of the Si-IV phase. The nanoindentation tip size and laser spot size were much smaller than the synthesized sample. During the nanoindentation and Raman measurements, we deliberately avoided the crack regions to prevent any potential influence on the experimental results.

The thermal conductivity of the metastable Si samples was measured using the optothermal Raman technique, where the laser excitation plays an essential role as the heat source. In brief, both temperature-dependent Raman shift $\mathrm{d}\omega/\mathrm{d}T$ and laser power-dependent Raman shift $\mathrm{d}\omega/\mathrm{d}P$ for one specific phonon mode of silicon are fundamental parameters to derive its thermal conductivity. In our case, all Raman spectra of silicon specimens were collected using a homemade Raman spectroscopy system equipped with an iHR550 spectrometer (Horiba, 1800 gr/mm grating) and a 50× objective lens (NA $\sim$ 0.75). The wavelength of the laser source was 532 nm, and its power density was accurately measured using a power meter (Thorlabs, S121C). Each Raman spectrum was acquired after the silicon sample reached thermal equilibrium with its surroundings. The laser power-dependent Raman measurements were performed at room temperature, and the laser power was tuned from 0.05 mW to 3.10 mW. The temperature-dependent Raman experiments were carried out in a homemade cryogenic setup, providing a wide base temperature range from 140 K to 300 K in a liquid nitrogen chamber. Meanwhile, the laser power was optimized to be below 0.4 mW, in order to minimize laser-induced heating effects. The typical integration time for each Raman curve was 50 s for Si-III/XII and 80 s for Si-IV.

Nanoindentation measurements of the metastable Si phases were performed using a nanoindenter apparatus (KLA G200) equipped with a Berkovich probe (correction factor $\beta \sim 1.034$), based on the continuous stiffness measurement technique. The maximum indentation depth was maintained to be far below 1/20 of the sample thickness, and a loading/unloading strain rate of 0.05 s^{-1} was applied throughout the experiments. The allowable thermal drift rate was 0.05 nm/s, and the actual thermal drift was measured and corrected at 90% unloading accordingly.

Crystal structures of the synthesized Si samples were characterized using advanced synchrotron x-ray diffraction (XRD) at the 15U1 beamline of the Shanghai Synchrotron Radiation Facility (SSRF). The wavelength of the x-ray beam was 0.6199 Å, and its spot size was focused within $\sim$ 3 μm. Two-dimensional diffraction images were captured with a MAR165 charge-coupled device (CCD) detector and subsequently integrated into one-dimensional XRD profiles using the Dioptas software.[23] The XRD data were further analyzed and refined using the Rietveld method implemented in GSAS-II.[24]

3. Results and discussion

The controlled preparation of metastable Si-III/XII and Si-IV phases can be achieved under high pressure via a diamond anvil cell, as reported in our previous study.[25] The Raman optothermal technique has been well developed to measure the thermal conductivity of functional materials, owing to its non-invasive and reliable features.[26] According to

Fourier's law, the heat flux ΔP, transmitted through an area A of a material, is proportional to its thermal conductivity κ and the negative temperature gradient $\mathrm{d}T/\mathrm{d}x$, i.e., $\Delta P/A = \kappa \mathrm{d}T/\mathrm{d}x$, where $A = \pi(a/2)^2$ corresponds to the heating area (laser source as the heater in our case), and thus a temperature gradient is generated. Therefore, thermal conductivity κ can be derived as $\kappa = \frac{2}{\pi a} \cdot \frac{\Delta P}{\Delta T}$. In practice, temperature-dependent Raman shift $\Delta\omega/\Delta T$ as well as laser power-dependent Raman shift $\Delta\omega/\Delta P$ can be obtained, leading to the experimental determination of thermal conductivity via $\kappa = \frac{2\cdot(\Delta\omega/\Delta T)}{\pi a\cdot(\Delta\omega/\Delta P)}$.[27] The spot size a of the laser beam can be accurately calibrated based on the knife-edge method, as depicted in Fig. S1.

We first investigated the thermal conductivity of the metastable Si-III/XII mixture using the Raman optothermal approach, as shown in Fig. 1. For this given metastable sample, the $I_{\text{Si-III}}/I_{\text{Si-XII}}$ ratio was determined to be around 0.68. Following lattice dynamics and group theory, it was found that the Si-III/XII mixture exhibits two sharp Raman peaks belonging to the A_g mode of Si-XII and E_u mode of Si-III, which appeared at ~ 353 cm^{-1} and ~ 435 cm^{-1} under low power excitation in our case (Fig. S2), respectively. In Fig. 1(a), the intensity of each Raman peak becomes remarkably stronger as the laser power increases. More importantly, all Raman peaks show a significant redshift with laser power due to the laser-induced heating effect. The linear slope $\mathrm{d}\omega/\mathrm{d}P$ of Raman shifts as a function of laser power was fitted as -0.80 cm^{-1}/mW and -0.71 cm^{-1}/mW for Si-XII A_g and Si-III E_u modes in Fig. 1(b), respectively. Within the laser power range explored in this experiment, the maximum Raman shifts approached ~ 2.2 cm^{-1} and ~ 2.1 cm^{-1} for Si-XII and Si-III phases, respectively, indicating a local temperature rise of about 80 K.[28] In principle, the phonon energy of the silicon lattice becomes weakened at high temperatures, owing to the prominent thermal expansion and anharmonic characteristics of the interatomic potential. This phenomenon occurred in Fig. 1(c), where the sample temperature varied from 310 K to 250 K in a liquid nitrogen chamber. Moreover, Raman shifts of both Si-XII A_g and Si-III E_u modes vary linearly within this temperature range. Therefore, the linear fitting process is reasonable, leading to a similar slope $\mathrm{d}\omega/\mathrm{d}T$ of -0.03 cm^{-1}/K for Si-XII A_g and Si-III E_u modes, as displayed in Fig. 1(d). As discussed above, the phenomenological thermal conductivities $\kappa_{\text{Si-XII}}$ and $\kappa_{\text{Si-III}}$ were calculated to be 33.2 W·m^{-1}·K^{-1} and 37.4 W·m^{-1}·K^{-1}, respectively.

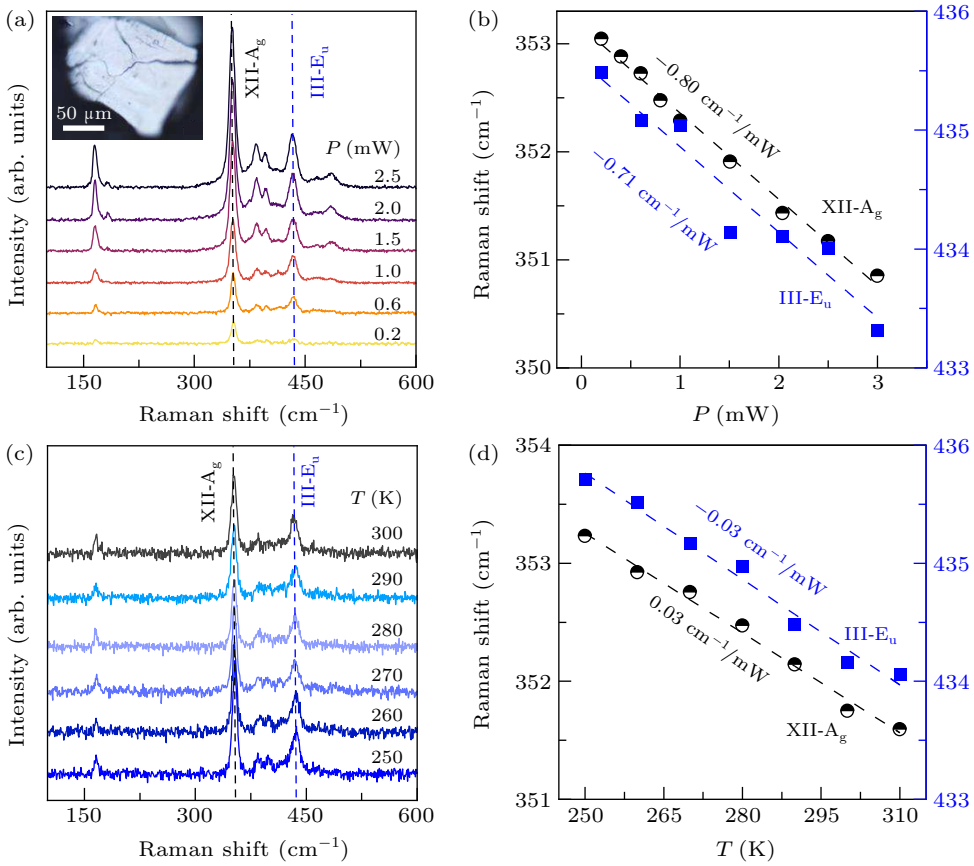


Fig. 1. Thermal conductivity measurement of Si-III/XII mixture based on Raman optothermal technique. (a) The obtained Raman spectra of Si-III/XII with varying laser powers. The inset shows the representative optical image of the Si-III/XII sample. The dashed lines indicate the A_g mode of Si-XII (black) and E_u mode of Si-III (blue), observed at 353.0 cm^{-1} and 435.5 cm^{-1} under 0.2 mW, respectively. (b) Laser power-dependent Raman A_g mode of Si-XII (black) and E_u mode of Si-III phase (blue). The dashed lines represent the linear fitting results. (c) Raman spectra of Si-III/XII measured at different temperatures from 300 K down to 250 K. (d) Temperature-dependent Raman A_g mode of Si-XII (black) and E_u mode of Si-III phase (blue). The $I_{\text{Si-III}}/I_{\text{Si-XII}}$ ratio of this measured Si-III/XII sample was around 0.68.

Furthermore, the nominal thermal conductivities of multiple Si-III/XII mixtures with various $I_{\text{Si-III}}/I_{\text{Si-XII}}$ ratios were systematically measured to elucidate their dependence on phase concentration. It is worth noting that the total thermal conductivity of a mixture or alloy is generally lower than that of each pure constituent due to the broken phonon coherence and its reduced mean free path.[29,30] As established in our earlier study,[25] the dynamic decompression process plays a significant role in modulating the Si-III to Si-XII ratio. As shown in Fig. S3, the phenomenological thermal conductivities of both Si-III and Si-XII phases monotonically decrease as the proportion of Si-III phase increases, potentially suggesting that pure Si-XII has a higher thermal conductivity than Si-III. First-principles calculations predict that the anisotropic thermal conductivity of pure Si-XII is 16.8 $\text{W}\cdot\text{m}^{-1}\cdot\text{K}^{-1}$ and 8.9 $\text{W}\cdot\text{m}^{-1}\cdot\text{K}^{-1}$ along the x and z axes, respectively,[18] while the measured thermal conductivity of the Si-III phase is 20 $\text{W}\cdot\text{m}^{-1}\cdot\text{K}^{-1}$ at 300 K,[15] which are close to those of Si-III/XII mixtures with an $I_{\text{Si-III}}/I_{\text{Si-XII}}$ ratio over ~ 0.8 in our case.

Next, we investigated the thermal conductivity of the Si-IV phase using the Raman optothermal approach, as shown in Fig. 2. The pure Si-IV phase was efficiently obtained by thermal annealing of Si-III/XII and further confirmed by synchrotron x-ray diffraction measurements (Fig. S4).[25] Figure 2(a) exhibits the acquired Raman spectra of Si-IV under variable laser powers up to 3.10 mW. For each curve, there is only one asymmetric and broad Raman band, which can be well fitted with two Lorentzian peaks at ~ 482 cm^{-1} and 517 cm^{-1} (0.25 mW), corresponding to the E_{2g} and E_{1g} phonon modes of the Si-IV phase (Fig. S5).[31] The latter E_{1g} mode was selected to analyze the thermal conductivity of the Si-IV phase due to its relatively stronger intensity. The correlation between E_{1g} energy and laser power was found to approximate a linear function with $\text{d}\omega/\text{d}P \sim -1.11$ cm^{-1}/mW, as displayed in Fig. 2(b). Similarly, Figs. 2(c) and 2(d) present the linear dependence of Raman shift on temperature, and the linear slope $\text{d}\omega/\text{d}T$ was extracted as -0.04 cm^{-1}/K. Therefore, the thermal conductivity of the Si-IV phase was calculated to be 31.9 $\text{W}\cdot\text{m}^{-1}\cdot\text{K}^{-1}$, superior to those of Si-III and Si-XII phases, especially for $I_{\text{Si-III}}/I_{\text{Si-XII}} > \sim 0.75$ in Fig. S3. Notably, our experimental result is significantly lower than the theoretical value of 74 $\text{W}\cdot\text{m}^{-1}\cdot\text{K}^{-1}$ at 300 K.[20] This discrepancy arises due to the polycrystalline nature of our Si-IV sample, where structural defects, such as grain boundaries and dislocations induced under high pressure, can dramatically scatter phonon transport and hence degrade its thermal conductance.[32]

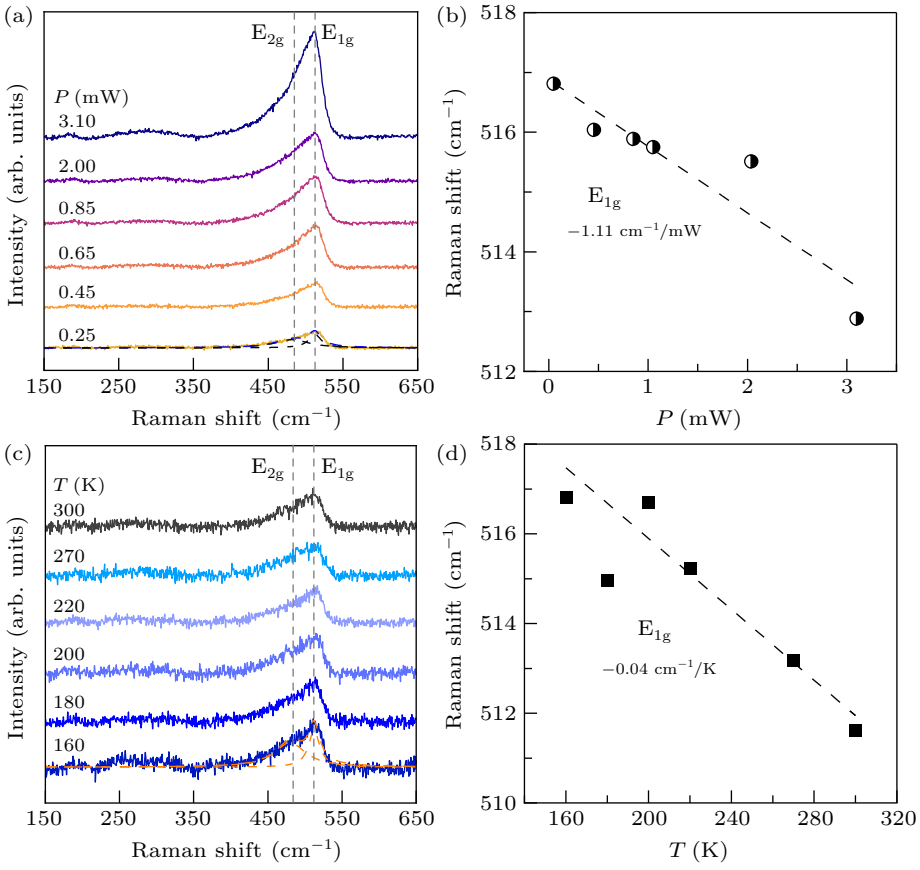


Fig. 2. Thermal conductivity measurement of Si-IV phase based on Raman optothermal technique. (a) Raman spectra of Si-IV at different power levels. (b) The relationship between Raman E_{1g} mode of Si-IV and laser power. (c) Raman spectra of Si-IV acquired at different temperatures. (d) The relationship between Raman E_{1g} mode of Si-IV and temperature. The dashed lines represent the linear fitting results.

Thermal conductivity tests were systematically carried out on Si-III, Si-XII, and Si-IV phases, along with the pristine and high-pressure treated Si-I samples, in an attempt to uncover the underlying mechanisms. The obtained thermal conductivities of the metastable phases are summarized in Fig. 3, combined with literature data.[15,18,20,33–37] We measured the thermal conductivity of pristine Si-I to be 139 $W{\cdot}m^{-1}{\cdot}K^{-1}$ at 300 K (the raw data shown in Figs. S6–S8), which is consistent with the literature values of 156 $W{\cdot}m^{-1}{\cdot}K^{-1}$,[35] 142 $W{\cdot}m^{-1}{\cdot}K^{-1}$,[36] 125 $W{\cdot}m^{-1}{\cdot}K^{-1}$,[34] and 120 $W{\cdot}m^{-1}{\cdot}K^{-1}$.[37] Due to inherent differences in measurement techniques and variations in sample quality, some deviations between our results and the literature are expected, but all fall within an acceptable error range. In particular, the excellent agreement between our result (139 $W{\cdot}m^{-1}{\cdot}K^{-1}$) and the reported value of 142 $W{\cdot}m^{-1}{\cdot}K^{-1}$ further supports the reliability of our experimental data. It is evident that high-pressure treatment can dramatically reduce the thermal conductivity of pristine Si-I, from the initial 139 to 9.6 $W{\cdot}m^{-1}{\cdot}K^{-1}$ after 8 GPa, as an example. Moreover, these comparative analyses also confirm that the relatively low thermal conductivity of Si-III/XII and Si-IV phases transformed from Si-I under high pressure. In principle, the thermal conductivity of metastable Si phases is governed by phonon transport behavior, and their electronic contribution can be considered negligible, due to their semiconducting characteristics. Numerous structural defects emerge in the silicon lattice under extreme pressure and can even be retained under ambient conditions, which create numerous scattering centers with lattice phonons. Based on the modified Callaway model, we know that phonon lifetime τ is rapidly shortened by their inelastic interactions with point ($\tau^{-1} \sim \omega^4$), dislocation ($\tau^{-1} \sim \omega^3$), and boundary ($\tau^{-1} \sim \omega$) defects, where ω is the phonon angular frequency.[38] Importantly, thermal annealing can efficiently reconstruct the atomic arrangement, thereby eliminating lattice defects and resulting in gradually enhanced thermal conductivity. This phenomenon was clearly demonstrated in our annealed Si-I at 1273 K for 10 hours, with its thermal conductivity raised to 13.4 $W{\cdot}m^{-1}{\cdot}K^{-1}$. It is worth noting that, to simplify the calculation, the absorption of the materials is not considered in the thermal conductivity calculation, which may affect ΔP and consequently lead to some deviation in the results.[26] In addition, at room temperature, the thermal conductivity of amorphous silicon approximates 1.8 $W{\cdot}m^{-1}{\cdot}K^{-1}$,[39] while that of amorphous silicon thin films is less than 0.03 $W{\cdot}m^{-1}{\cdot}K^{-1}$.[40] Obviously, the thermal conductivity of silicon films is much lower than that of bulk Si-I and decreases further with decreasing thickness.[41]

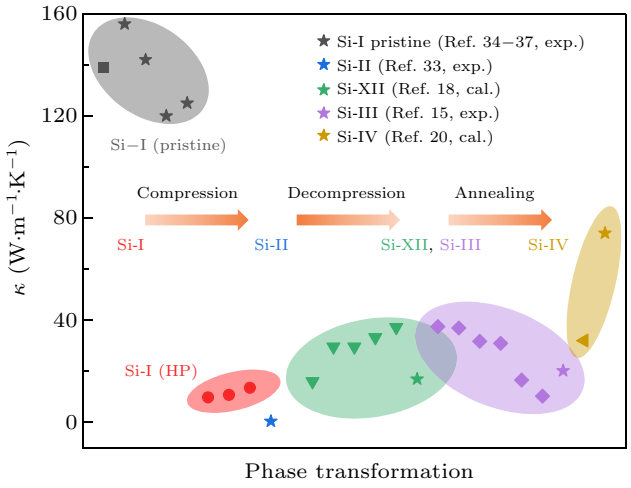


Fig. 3. Thermal conductivity of Si in various phases, including Si-I, Si-II, Si-XII, Si-III, and Si-IV. The inset illustrates the transition pathways of silicon. Data points marked with stars represent the literature results.

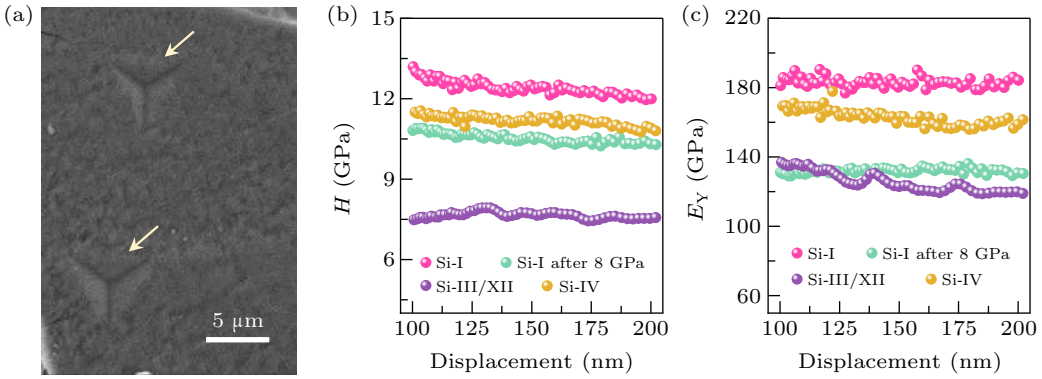


Fig. 4. Hardness and Young's modulus measurements of various silicon phases using the nanoindentation technique. (a) Scanning electron microscope image of Si-III/XII after the nanoindentation test, with the indented areas marked by two arrows. (b) Relationship between hardness H and displacement for single-crystalline Si-I, polycrystalline Si-I, Si-III/XII, and Si-IV phases. (c) Relationship between Young's modulus E_Y and displacement for single-crystalline Si-I, polycrystalline Si-I, Si-III/XII, and Si-IV phases.

Next, we turn to examine the mechanical hardness H and Young's modulus E_Y of metastable Si phases using the nanoindentation method,[42] including the Si-III/XII mixture and Si-IV, compared with pristine Si-I and decompressed Si-I from 8 GPa. The representative load-displacement curves of each phase in Fig. S9 show good repeatability, indicating reliable

mechanical results. The extracted hardness and Young's modulus results are shown in Fig. 4. The mean H and E_Y of the pristine Si-I phase are 12.1 ± 0.5 GPa and 183.5 ± 5.2 GPa, respectively, which are consistent with literature data.[43] Once subjected to high pressure, the mechanical properties of the Si-I phase were remarkably degraded, with $E_Y \sim 138.3 \pm 7.1$ GPa after 8 GPa. This phenomenon can be well explained by the pressure-induced lattice defects.[22] In comparison, the hardness and Young's modulus of Si-III/XII and Si-IV are approximately 35% and 15% lower than those of the Si-I phase, respectively.

In detail, all Si allotropes are covalently connected with sp^3 hybridized bonds. According to Rietveld refinements of XRD results, both hexagonal Si-IV (2.33 Å and 2.37 Å) and body-centered Si-III (2.34 Å and 2.39 Å) lattices have two distinct Si–Si bond lengths, whereas the rhombohedral Si-XII phase shares four longer bond lengths: 2.38 Å, 2.40 Å, 2.34 Å, and 2.38 Å. Therefore, the comparable modulus of Si-IV and Si-I originates from their similar atomic bond characteristics, both of which are stronger than that of the Si-III/XII mixture.

We further summarized the hardness and Young's modulus of various Si phases in Fig. 5. Clearly, the mechanical properties of Si show notable tunability, depending on the specific phase structure. For instance, the hardness can vary from 7.4 ± 0.7 GPa (Si-III/XII) to 12.1 ± 0.5 GPa (Si-I), enabling the fabrication of all Si-based mechanical sensors. Our obtained hardness and elastic modulus results for the Si-IV phase are quantitatively comparable with those of cubic Si-I, consistent with the literature data,[21] where the bulk modulus is ~ 91.8 GPa and Poisson's ratio is ~ 0.22. All metastable Si phases exhibit brittle characteristics due to their robust covalent bonds. The nanoindentation process induces irreversible plastic deformation on the silicon surface, as illustrated in Fig. 4(a). The structural defects caused by extreme pressure can significantly weaken the mechanical strength of silicon due to pronounced surface and size effects, as evidenced by our Si-I phase, which cannot be intuitively predicted by standard continuum mechanics.[44,45]

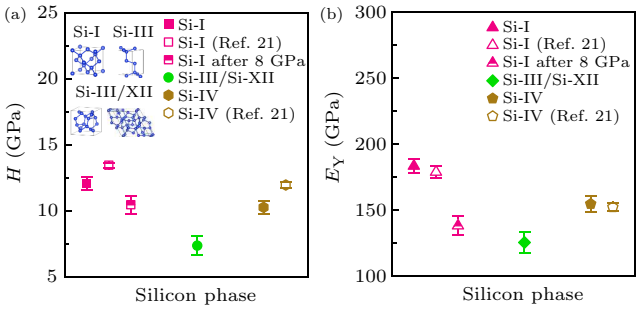


Fig. 5. Phase structure-dependent mechanical properties of silicon. (a) Hardness H of silicon, with the lattice structure of each silicon phase shown in the inset. (b) Young's modulus E_Y of silicon.

4. Conclusion

In summary, the phase structure-regulated thermal and mechanical properties of metastable silicon have been systematically investigated. It was found that the thermal conductivities of Si-III and Si-XII are highly sensitive to their phase concentration, and the thermal conductivity of polycrystalline Si-IV (31.9 $W \cdot m^{-1} \cdot K^{-1}$) is much lower than that of Si-I, partially due to the prominent phonon-defect scattering effect. Nanoindentation characterization revealed that the hardness and Young's modulus of Si-III/XII ($H \sim 7.4 \pm 0.7$ GPa and $E_Y \sim 125.7 \pm 8.1$ GPa) and Si-IV ($H \sim 10.3 \pm 0.5$ GPa and $E_Y \sim 154.8 \pm 5.9$ GPa) phases are significantly lower than those of the cubic Si-I phase. These findings are expected to open new avenues for exploring the distinguished properties of novel Si allotropes and further expand their practical applications beyond the typical cubic Si-I counterpart.

Acknowledgments

This project was supported by the National Natural Science Foundation of China (Grant Nos. 52472040, 52072032, and 12090031) and the 173 JCJQ program (Grant No. 2021-JCJQ-JJ-0159). We gratefully thank Dr. H.L. Dong for his support with the synchrotron XRD measurements.

References

[1] Ballif C, Haug F J, Boccard M, Verlinden P J and Hahn G 2022 *Nat. Rev. Mater.* **7** 597
[2] Shekhar S, Bogaerts W, Chrostowski L, Bowers J E, Hochberg M, Soref R and Shastri B J 2024 *Nat. Commun.* **15** 751
[3] Barth S, Seifner M S and Maldonado S 2020 *Chem. Mater.* **32** 2703
[4] Franco Gonzalez A, Yang N H and Liu R S 2017 *J. Phys. Chem. C* **121** 27775
[5] Fadaly E M T, Dijkstra A, Suckert J R, *et al.* 2020 *Nature* **580** 205
[6] Zhang L, Wang Y, Lv J and Ma Y 2017 *Nat. Rev. Mater.* **2** 17005
[7] Mujica A, Rubio A, Munoz A and Needs R 2003 *Rev. Mod. Phys.* **75** 863
[8] Ge G, Rovaris F, Lanzoni D, Barbisan L, Tang X, Miglio L, Marzegalli A, Scalise E and Montalenti F 2024 *Acta. Mater.* **263** 119465
[9] Anzellini S, Wharmby M T, Miozzi F, Kleppe A, Daisenberger D and Wilhelm H 2019 *Sci. Rep.* **9** 15537
[10] Wippermann S, He Y, Vörös M and Galli G 2016 *Appl. Phys. Rev.* **3** 040807
[11] Kailer A, Gogotsi Y G and Nickel K G 1997 *J. Appl. Phys.* **81** 3057
[12] Piltz R, Maclean J, Clark S, Ackland G, Hatton P and Crain J 1995 *Phys. Rev. B* **52** 4072
[13] Shiell T B, Zhu L, Cook B A, Bradby J E, Mcculloch D G and Strobel T A 2021 *Phys. Rev. Lett.* **126** 215701
[14] Wong S, Johnson B C, Haberl B, Mujica A, Mccallum J C, Williams J S and Bradby J E 2019 *J. Appl. Phys.* **126** 105901
[15] Zhang H, Liu H, Wei K, Kurakevych O O, Le Godec Y, Liu Z, Martin J, Guerrette M, Nolas G S and Strobel T A 2017 *Phys. Rev. Lett.* **118** 146601
[16] Ci P, Sun M, Upadhyaya M, Song H, Jin L, Sun B, Jones M R, Ager J W, Aksamija Z and Wu J 2022 *Phys. Rev. Lett.* **128** 085901
[17] Zhou Y, Dong Z Y, Hsieh W P, Goncharov A F and Chen X J 2022 *Nat. Rev. Phys.* **4** 319
[18] Rao Y, Zhao C Y and Ju S 2022 *Appl. Phys. Lett.* **120** 163901
[19] Harish S, Tabara M, Ikoma Y, Horita Z, Takata Y, Cahill D G and Kohno M 2014 *Nanoscale Res. Lett.* **9** 326

[20] Raya-Moreno M, Aramberri H, Seijas-Bellido J A, Cartoix'a X and Rurali R 2017 *Appl. Phys. Lett.* **111** 032107

[21] Liang T, Xiong L, Lou H, Lan F, Zhang J, Liu Y, Li D, Zeng Q and Zeng Z 2022 *Scripta Mater.* **220** 114936

[22] Kim H S and Bush M B 1999 *Nanostruct. Mater.* **11** 361

[23] Prescher C and Prakapenka V B 2015 *High Pressure Res.* **35** 223

[24] Toby B H and Von Dreele R B 2013 *J. Appl. Crystallogr.* **46** 544

[25] Du Y, Du G, Dong H, Li J, Han W, Chen B and Chen Y 2024 *J. Phys. Chem. C* **128** 4818

[26] Balandin A A, Ghosh S, Bao W, Calizo I, Teweldebrhan D, Miao F and Lau C N 2008 *Nano Lett.* **8** 902

[27] Gan Y L, Wang L, Su X Q, Xu S W, Shen X and Wang R P 2014 *J. Raman Spectrosc.* **45** 377

[28] Johnson B C, Haberl B, Bradby J E, Mccallum J C and Williams J S 2011 *Phys. Rev. B* **83** 235205

[29] Zhou J, Liao B and Chen G 2016 *Semicond. Sci. Technol.* **31** 043001

[30] Abeles B 1963 *Phys. Rev.* **131** 1906

[31] Dixit S and Shukla A K 2018 *J. Appl. Phys.* **123** 224301

[32] Ikoma Y, Hayano K, Edalati K, Saito K, Guo Q and Horita Z 2012 *Appl. Phys. Lett.* **101** 121908

[33] Abdel-Aal H A, Reyes Y, Patten J A and Dong L 2006 *Mater. Charact.* **57** 281

[34] Cao F and He Z 2022 *Int. J. Mod. Phys. B* **36** 2240050

[35] Glassbrenner C J and Slack G A 1964 *Phys. Rev.* **134** A1058

[36] Shanks H R, Maycock P D, Sidles P H and Danielson G C 1963 *Phys. Rev.* **130** 1743

[37] Pfeifer T W, Tomko J A, Hoglund E, Scott E A, Hattar K, Huynh K, Liao M, Goorsky M and Hopkins P E 2022 *J. Appl. Phys.* **132** 075112

[38] Cahill D G, Braun P V, Chen G, Clarke D R, Fan S, Goodson K E, Keblinski P, King W P, Mahan G D, Majumdar A, Maris H J, Phillpot S R, Pop E and Shi L 2014 *Appl. Phys. Rev.* **1** 011305

[39] Hiroshi Wada H W and Takeshi Kamijoh T K 1996 *Jpn. J. Appl. Phys.* **35** L648

[40] Zink B L, Pietri R and Hellman F 2006 *Phys. Rev. Lett.* **96** 055902

[41] Jeong C, Datta S and Lundstrom M 2012 *J. Appl. Phys.* **111** 093708

[42] Li X and Bhushan B 2002 *Mater. Charact.* **48** 11

[43] Pharr G M, Oliver W C and Clarke D R 1990 *J. Electron. Mater.* **19** 881

[44] Ronald E M and Vijay B S 2000 *Nanotechnol.* **11** 139

[45] Sadeghian H, Yang C K, Goosen J F L, Bossche A, Staufer U, French P J and Van Keulen F 2010 *J. Micromech. Microeng.* **20** 064012